This is a preprint version of the paper published in Thermochimica Acta, Volume 683, January 2020, 178430, doi: 10.1016/j.tca.2019.178430

Thermal decomposition of cerium triethanolamine complexes

Imen Zghal[1,2], Jordi Farjas[1], Jaume Camps[1], Mohamed Dammak[2], Pere Roura-Grabulosa[1].

[1]University of Girona, Campus Montilivi, Edif. PII, E17071 Girona, Catalonia, Spain

[2]Laboratoire de Chimie Inorganique, Faculté des Sciences de Sfax, University of Sfax, BP 1171, 3000 Sfax, Tunisia

Abstract

Thermal decomposition of cerium triethanolamine complexes to cerium oxide, CeO_2, in inert and oxidative atmospheres has been investigated by thermogravimetry combined with infrared evolved gas analysis; the main volatiles formed during thermal decomposition have been identified. Intermediates and final products have been characterized by infrared spectroscopy, X-Ray diffraction and elemental analysis. Several overlapping steps occurring along decomposition path have been identified and plausible reaction pathways are presented. It will be shown that decomposition starts around 200ºC independently of the atmosphere, but the endset temperature depends on the gas composition: the more inert the atmosphere the higher the endset temperature. Finally, the effect of the temperature and amount of triethanolamine used during compound synthesis is discussed.

Keywords: CeO_2, Thermal decomposition, TGA-EGA, Pyrolysis, triethanolamine metal complex.

*Corresponding author: jordi.farjas@udg.cat, Tel (34)972418490, Fax (34) 972418098
University of Girona, Campus Montilivi, Edif. PII, E17003 Girona, Catalonia, Spain

1. Introduction

Cerium(IV) oxide (ceria), CeO_2 possesses good mechanical, chemical and thermal stability. Ceria has been extensively used as catalyst [1,2], electrolyte for solid-oxide fuel cells [3], oxygen sensors [4], UV-protecting coating [5,6], anticorrosion coating in metals [7], abrasive in chemical–mechanical polishing [8] and as buffer layer for coated superconductor architectures [9,10].

Among the available CeO_2 synthesis routes, combustion synthesis is commonly used because it is straightforward and low-cost [2,11–15]. Taking advantage of the heat released during precursor decomposition, product formation is achieved at low processing temperature in a very short time lapse. Besides, triethanolamine (TEA) has been successfully used as a chelating agent to obtain stable crystalline 3d–4f–heterometallic complexes [12,16–26]. TEA–nitrate–metal complexes are of special interest as precursors for combustion synthesis because TEA is a reducing agent while the nitrate group is a strong oxidizing agent. So these compounds contain both the fuel and the oxidizer needed to sustain combustion. Several Ce–TEA compounds easily undergo a thermal runaway [19] and have been used as precursors for combustion synthesis of ceria [2,12,27]

In general, the thermal decomposition of TEA–metal complexes is a process that spans a temperature interval larger than 100ºC and involves several stages [19,23,28]. Ce–TEA complex in air and nitrogen dynamic atmospheres melts at 169ºC and decomposes abruptly through a very exothermic process around 200ºC [19]. The occurrence of a thermal runaway hides the complex behavior of Ce–TEA during decomposition. In the event of a thermal runaway, Ce–TEA decomposition ends at around 400ºC yielding crystalline ceria but, as far as we know, no analysis of the evolved gases has been performed. Thus, there is no information about the decomposition mechanism as well as the volatiles formed during its decomposition.

Analysis of the mechanisms involved in thermal decomposition as well as identification of the volatiles evolved are crucial to gain a better understanding of the processes that take place in view to optimize CeO_2 synthesis. The aim of this paper is to analyze the thermal decomposition of two cerium triethanolamine complexes to yield CeO_2. To analyze the evolution during thermal decomposition, thermogravimetry and in-situ infrared evolved gas analysis has been done under inert and oxidative atmospheres. In addition, quenches at selected temperatures have been performed to analyze solid

intermediates by Fast Fourier Infrared spectroscopy (FTIR), X-Ray diffraction (XRD) and Elemental Analysis (EA).

2. Materials and methods

2.1 Preparation of Ce–TEA complexes

Samples were prepared dissolving Cerium(III) nitrate hexahydrate ($Ce(NO_3)_3 \cdot 6H_2O$ Alfa Aesar ≥ 99.5%) into a mixture of 1−propanol (VWR, ≥ 99.9%) and triethanolamine (TEA, $C_6H_{15}NO_3$, Merck, ≥99%). Two different precursors have been synthetized.

Compound Ce−TEA−1 was obtained following the procedure described in ref. [12]. A mixture of 10.86 g of cerium nitrate, 3.736 g of triethanolamine and 200 ml of 1−propanol was stirred under nitrogen flow during 5 hours at a temperature of 97ºC (boiling point of 1−propanol). Then the mixture was filtered and the resulting crystals were washed successively in ethanol and acetone. Finally, the crystals were dried at room temperature in vacuum.

Synthesis of compound Ce−TEA−2 followed the procedure reported in ref. [19]. A solution of 10.86 g of cerium nitrate in 200 ml 1−propanol was obtained in a round bottom flask after stirring under nitrogen at 60ºC using a stirring magnetic hot plate. Afterwards, the heating system was shut down and simultaneously a mixture of 7.472 g of TEA in 100 ml of 1−propanol was added to the warm cerium nitrate solution. This mixture was stirred under nitrogen for 30 minutes. Afterwards the sample was washed and dried following the same procedure used for Ce−TEA−1.

Note that, in the mixture used to obtain Ce−TEA−1, the molar ratio Ce nitrate: TEA was close to 1:1 while, for Ce−TEA−2, it was approximately 1:2.

2.2 Characterization techniques

Simultaneous thermogravimetric (TG) and Differential Scanning Calorimetry (DSC) analyses were performed in a Mettler Toledo thermo-balance, model TGA/DSC1, at 10°C/min under a gas flow of 40 ml/min of high purity N_2 (Praxair, ≥99.999%) or synthetic air. Uncovered Al_2O_3 pans of 350 µl were used. To simultaneously monitor the evolution of the volatiles during precursor decomposition, Evolved Gas Analysis (EGA) was performed by coupling the TG furnace to of a Fourier–Transform infrared (FTIR) Gas Analyzer Bruker ALPHA model. A 40 cm long steel tube kept at 200°C was used to

connect the TG gas exhaust to the IR gas cell. A FTIR spectrum is recorded each 35 s with a wavenumber step of 2 cm^{-1}. DSC analysis was carried out in a Mettler Toledo DSC821e; samples of around 2 mg were placed inside 40 µl aluminum pans that were covered with a pierced lid to allow gas exchange. DSC measurements were done under a constant heating rate of 10°C/min and under a gas flow of 40 ml/min of high purity N_2. The maximum temperatures of the TG and DSC measurements were 850 and 640ºC respectively.

X–ray diffraction (XRD) spectrums were obtained using a D8 ADVANCE diffractometer from Bruker AXS with a Cu–Kα source (1.5406 Å) operating at 40 kV and 40 mA. IR analysis of solid samples was done by FTIR Spectrometry (Bruker model ALPHA) equipped with an attenuated total reflection (ATR) unit (model Platinum). Finally, Elemental Analysis (EA) was carried out on a Perkin Elmer 2400 series elemental analyzer.

3. Results and discussion

3.1 Characterization of the initial compounds and final product

The XRD curve of Ce−TEA−2 (Fig. 1) perfectly fits the structure of $[La(NO_3)(C_6H_{15}NO_3)_2](NO_3)_2$ [21]; a network of $[La(NO_3)(C_6H_{15}NO_3)_2]^{2+}$ cations and nitrate counter-ions (a similar structure was also reported for Pr as metal [22]). In this structure, TEA acts as a tetradentate ligand [24], a nitrate group is bonded to the Ce atom in bidentate mode, and two nitrate groups, that are not coordinated, compensate the charge of the cation. In addition, EA analysis of the compound Ce−TEA−2 agrees with the expected values for the Ce(III) complex: $[Ce(NO_3)(C_6H_{15}NO_3)_2](NO_3)_2$ (see Table 1) and those reported in ref. [19]. Furthermore, the FTIR analysis of Ce−TEA−2 (Fig. 2 and Table 2) shows the presence of absorption bands related to the OH groups (3157, 1641, 1596, 1325 and 667 cm^{-1}), to the CH_2 groups (2990, 2970, 2908, 2855 and 1378 cm^{-1}), to N−O (1135 cm^{-1}), non-coordinated NO_3 groups (1435 cm^{-1}) and coordinated bidentate NO_3 group (1460 and 1290 cm^{-1}, N=O and N−O stretching, respectively) [29]. The difference of the two absorption bands (approx. 170 cm^{-1}) is very close to 180 cm^{-1}, a typical value for bidentate nitrato chelating groups [29].

Finally, the relative mass of the residue after complete decomposition (Fig. 3) coincides with the mass expected for the transformation of $[Ce(NO_3)(C_6H_{15}NO_3)_2](NO_3)_2$ into CeO_2:

$$\frac{m(CeO_2)}{m([Ce(NO_3)(C_6H_{15}NO_3)_2](NO_3)_2)} \times 100 = 27.6\%$$

The formation of ceria as final product has also been confirmed by XRD (inset Fig. 1). CeO_2 is always the decomposition product of Ce−TEA−1 and Ce−TEA−2 either in air or in N_2.

The structure of Ce−TEA−1 differs significantly from that of Ce−TEA−2 as revealed by XRD (Fig. 1) and by FTIR (Fig. 2). The presence of strong diffraction peaks at low angles ($2\theta<10^o$) can be attributed to a Ce(IV)−TEA compound [29]. The lack of absorption bands related to OH groups in as-grown Ce−TEA−1 compound indicates that TEA is deprotonated. Moreover, the absorption bands related to CH_2 groups, to N−O and to C−C−O vibrations already observed in Ce−TEA−2 are still present, but they are less intense, indicating that the organic fraction is smaller in Ce−TEA−1. The latter fact is also supported by TG and EA. For Ce−TEA−1, the ratio between the final and initial masses is 57.0% (i.e. around twice the ratio between the final and initial masses for Ce−TEA−2). EA results make also clear that the amount of carbon, hydrogen and nitrogen is lower in Ce−TEA−1 than in Ce−TEA−2 (Tables 1 and 3).

It is known that deprotonated TEA forms stable atrane structures [25,26] where the three deprotonated oxygen atoms of TEA are directly coordinated to the metal. The deprotonated oxygen atoms of TEA can also coordinate to a neighboring cerium. In this case, a complex is formed [26]. Indeed, Wattanathana et al. [12] have analyzed the structure of Ce−TEA−2 by means of electrospray ionization and they have proposed three possible structures in which a cerium atom is bonded to a deprotonated TEA that acts as a tridentate ligand. The differences between the Ce−TEA−1 and Ce−TEA−2 result mostly from the fact they have been prepared using a Ce/TEA molar ratio of 1:1 and 1:2, respectively. Indeed, 1:1 reactions between TEA and lanthanide nitrates promote the formation of complexes with a metal/TEA molar ratio of 1:1 where TEA deprotonates, whereas an excess of TEA prevents TEA deprotonation and favors the formation of complexes like Ce−TEA−2 [22].

Therefore, and taking into account that FTIR reveals that TEA has been fully deprotonated, Ce−TEA−1 may be described as $Ce(C_6H_{12}NO_3)(NO_3)_x$. However, this formula is not compatible with EA results and the mass loss measured by TG. This contradiction can be solved if we take into account that nanocrystalline ceria precipitation has been reported in a solution of cerium nitrate and TEA in 1−propanol [30]. Moreover, increasing the temperature enhances the formation of ceria [29]: therefore, one could

expect that Ce−TEA−1 is a mixture of a Ce−TEA complex and ceria. The presence of ceria is also supported by the presence of an absorption peak at 462 cm^{-1} that is characteristic of the Ce−O bond. Assuming that Ce−TEA−1 is a mixture of a Ce−TEA compound and ceria, and knowing from EA the carbon and nitrogen contents (Table 3), we have calculated the composition of Ce−TEA−1. The result is $Ce(C_6H_{12}NO_3)(NO_3)_{1.21}$+0.56 CeO_2. This composition leads to a predicted H content of 2.57%, which is in fair agreement with the amount measured by EA, 2.45%. Also, we have calculated the ratio between the masses of CeO_2 and $Ce(C_6H_{12}NO_3)(NO_3)_{1.21}$+0.56 CeO_2. This ratio (58.7%) is in fair agreement with the normalized mass determined from TG (57.0% in Fig. 3). Since Ce−TEA−1 is a mixture of two compounds, its composition is not fixed; small variations of the synthesis time or temperature results in a different amount of ceria. Indeed, EA and TG measurements of different batches show little deviations on the composition of the mixture while a perfect reproducibility was always obtained for Ce−TEA−2.

The FTIR analysis of Ce−TEA−1 shows that the absorption bands related to coordinated NO_3 are absent and only the absorption band of non-coordinated NO_3 is present (1413 cm^{-1}) [31]. Its shift to lower wavenumbers indicates that it is weakly bonded to the cation. The presence of non-coordinated NO_3 can be interpreted as counter-ions for the $[Ce(C_6H_{12}NO_3)]^+$ cations. The existence of $[Ce(C_6H_{12}NO_3)]^+$ cations indicates that Ce(III) of the hydrated nitrate used for synthesis has been transformed to Ce(IV) in Ce−TEA−1. Probably, the deprotonation of the TEA oxygen atoms is related to this change. Furthermore, the formation of a Ce(IV)−TEA compound may further enhance the formation of CeO_2 [29].

3.2 First steps of thermal evolution: melting and 1−propanol evolution.

From the DSC curves obtained under air or N_2, Fig. 3, the first thermal event observed is the melting of the Ce−TEA−2 compound at 169ºC (onset temperature). The same melting temperature has been reported in N_2 and air by Içbudak et al. [19]. DSC measurements have deliver a melting enthalpy of 110±10 kJ/kg. Two consecutive DSC measurements done between 50 and 200ºC have confirmed that this transformation is reversible. The FTIR spectra (Fig. 2) of the as-ground compound and of a quenched sample heated up to 200ºC (above the melting process) are virtually identical, i.e., no degradation is apparent from FTIR analysis. Finally, visual inspection has confirmed the

occurrence of a melting process. According to ref. [21], $[Ce(NO_3)(C_6H_{15}NO_3)_2]^{2+}$ cations are bonded to their neighbors by a pair of bridging nitrate groups, OH groups of TEA make a near hydrogen bond to two non-coordinated nitrate groups. Thus melting of Ce−TEA−2 could be attributed to the collapse of these hydrogen like bonds. Conversely, since Ce−TEA−1 is not a pure substance it has not a fixed melting point, depending on the batch the melting point changes from 154 to 162ºC (the melting point and peak width increase with the amount of ceria).

From the dTG (time derivative of TG, dm/dt) curve in Fig. 4 it is apparent that there is a peak centered at 174ºC that is related to a slight mass loss that occurs during the melting process; the sample mass at 180ºC, is 98.9%. The main volatile evolved (see spectra at 174ºC of Fig. 5) is 1−propanol, the solvent used in the preparation of Ce−TEA−2. Since 1−propanol boiling point is 97ºC, this means that some 1−propanol is coordinated to the compound and it is released when the compound melts. The peaks at 174ºC for TEA and NH_3 in Fig. 4 are artifacts; to trace the evolution of TEA and NH_3 we plot the IR intensities at 1075 and 964 cm^{-1} respectively. These two frequencies are near two intense absorption of 1−propanol (Fig. 5), thus these two peaks are related to the formation of 1−propanol instead of TEA or NH_3.

Finally, there is a continuous background signal related to the water accumulated at the cold points of the thermobalance. The release of water from the sample can only be detected when there is clear signal evolution above the background signal. From Fig. 4 it is clear that we can only asses the evolution of water from the sample around 269ºC.

3.3 Thermal decomposition between 200 and 300ºC: TEA deprotonation.

The first mass-loss step of Ce−TEA−2 starts just after melting and its onset is independent of the furnace atmosphere, i.e., it is not triggered by the presence of oxygen. Içbudak et al. [19] also reported similar onset temperatures in flowing air and N_2, 199 and 195ºC respectively for samples also heated at 10 K/min. Furthermore, the evolution of the decomposition depends critically on the mass of the sample. When the sample mass is above a critical value (around 8 mg) the decomposition undergoes a thermal runaway that is characterized by a discontinuity in the first derivative of the mass evolution, a sudden drop of the sample mass and a sharp exothermic peak [32–34]. When a thermal runaway occurs, most of the decomposition takes place in a very short time interval at nearly adiabatically conditions; i.e., the sample is not thermalized and the local

temperature may rise few hundreds Kelvins above the reference temperature measured by the TG. This is the case of the 15.4 mg sample in air and 10.4 mg sample in N_2 (Fig. 3) and the measurement reported by Içbudak et al. [19]. Under these circumstances, the different processes that take place during decomposition overlap, so it is impossible to disclose the different stages involved in the thermal decomposition. For this reason, the simultaneous TG−EGA analysis (Figs. 4 and 5) and the analysis of the evolution of the solid residue (Fig. 2) have been done for a smaller mass of around 6 mg. Besides, the DSC signal shows that in both N2 or air the decomposition is an exothermic reaction, a necessary condition for combustion synthesis.

The simultaneous TG−EGA analysis of Fig. 4 shows that the thermal decomposition of Ce−TEA−2 is a complex process as it involves several stages. The temperatures at which the rate of formation of a certain volatile is maximum is indicated in Fig. 4 and the corresponding FTIR spectrum are shown in Fig. 5. The absence of any plateau in the TG curve (Fig. 3) and the overlapping of the evolution of the different volatiles (Fig. 4) indicates that the different processes overlap and that there are no stable intermediates. Nevertheless, we have performed EA and FTIR analyses of samples quenched at selected temperatures (Fig. 2) to characterize the evolution of solid residue along the decomposition.

The thermal decomposition starts around 200ºC; FTIR spectra of the as-grown compound and of a sample quenched at 200ºC are nearly identical (Fig 2) with the exception of a shoulder at 3500 cm^{-1} that can be attribute to water uptake after the sample quench. The dTG curve of Fig 4 shows a broad peak between 200 and 300ºC. The mass loss during this temperature interval is 44,2%; it represents a 61% of the total mass loss that takes place during Ce−TEA−1 decomposition.

The first volatile detected is TEA, that reaches its peak temperature at 251ºC (Fig.4). Besides, between 200ºC and 300ºC the mass loss accounts 61% of the total mass loss, therefore, it is reasonable to assume that, during this first stage, at least one TEA molecule evolves per cerium atom.

Concerning the solid residue, its FTIR spectra (Fig. 2) shows a progressive decrease of the intensity of the absorption bands related to TEA groups. It is noteworthy that at 225 ºC the FTIR spectra of the solid residue of Ce−TEA−2 is quite similar to that of as-grown Ce−TEA−1 (Fig. 6). Moreover, from Fig. 2, it is apparent that at 260ºC the absorption bands related to OH groups (3157 cm^{-1}) of Ce−TEA−2 have almost vanished. Therefore, we conclude that, during the first decomposition stage, Ce−TEA−2 evolves

towards Ce−TEA−1 structure: one TEA molecule linked to cerium evolves while the other TEA molecule becomes deprotonated and forms a stable atrane structure with the three oxygen directly bonded to cerium. Nevertheless, there is a significant difference between as-grown Ce−TEA−1 and Ce−TEA−2 quenched at 225ºC; for the latter the absence of the absorption peak at 462 cm^{-1} indicates that no CeO_2 has been formed yet, while Ce−TEA−1 contains a significant amount of CeO_2. Thus, this first step can be described as,

$$\text{Ce-TEA-2} \rightarrow \text{Ce-TEA-1} + \text{TEA} \quad (3.1)$$

The removal of one TEA molecule and the deprotonation of the second one is not compatible with the evolution of the relative amount of carbon, hydrogen and nitrogen determined by EA (Table 2). Instead of decreasing, the relative amount of carbon increases from 225 to 280ºC. The increase of the carbon content during TEA evolution could be attributed to removal of NO_3 groups, as expected if the structure of Ce−TEA−1 is approached. This conclusion is further confirmed by a progressive decrease of the intensity of the absorption bands related to bonded and not bonded NO_3 groups (1460 and 1435 cm^{-1}). Therefore, it is reasonable to assume that the proton related to the deprotonation of TEA combines with a NO_3 group to form nitric acid,

$$NO_3^- + H^+ \rightarrow HNO_3 \quad (3.2)$$

Since TEA is fully deprotonated and only two NO_3 groups are removed, the remaining proton may react with the residual oxygen of the furnace to form water. Indeed, from Fig. 4 it is apparent the evolution of water during this first stage. Thus the overall process can be described as,

$$[Ce(NO_3)(C_6H_{15}NO_3)_2](NO_3)_2 + \frac{1}{4}O_2 \rightarrow Ce(C_6H_{12}NO_3)NO_3 + C_6H_{15}NO_3 + \frac{1}{2}H_2O + 2HNO_3 \quad (3.3)$$

Moreover, From Fig. 4 and the spectra taken at 251 and 269ºC of Fig 5, it is clear that the removal of NO_3 groups is accompanied by the formation of N_2O, NO, CO_2, NH_3 and H_2O while TEA evolution vanishes. Given the fact that TEA is a strong reducing agent, the evolved TEA reacts with nitric acid gas to form N_2O,

$$TEA + HNO_3 \rightarrow N_2O + CO_2 + H_2O + \text{other TEA oxidation products} \quad (3.4)$$

where NO, CO_2, NH_3 and H_2O are the main volatiles related to TEA oxidation.

The mass loss expected for the transformation (3.2) is 44,2% and it coincides with the observed mass loss up to 300ºC (Fig.3). Thus, this first stage results in the formation

of $Ce(C_6H_{12}NO_3)NO_3$ with, first, the release of TEA followed by CO_2, N_2O, NO and H_2O as main volatiles and involves a change of the oxidation state from Ce(III) to Ce(IV).

The expected relative amount of carbon, hydrogen and nitrogen for $Ce(C_6H_{12}NO_3)NO_3$ are 20.7%, 3.5% and 8.0%. This composition is roughly in between the compositions given by EA of samples quenched at 280 and 300ºC. However, nitrogen and hydrogen amounts are below the theoretical ones, meaning that, although the reaction between the TEA proton and the NO_3 group has reached completion, some TEA remains. At this point it is worth noting that at 300ºC the first stage of decomposition is not over: both the dTG and CO_2 signals in Fig 4 have not reach a zero value but a minimum, i.e., this stage overlaps with the following decomposition stage.

3.4 Thermal decomposition between 300 and 800ºC: CeO_2 formation.

In inert atmosphere, the Ce−TEA−2 precursor is not fully decomposed until 800ºC. Since, in the atrane structure the deprotonated TEA is tightly bonded to the cerium through the Ce−O bond, the TEA molecule breaks apart before it is detached. From the dTG−EGA analysis of Fig. 4, we can distinguish three different stages. A first stage between 300 and 450ºC that reaches its maximum decomposition rate around 371ºC. The main volatiles observed are NH_3, CO_2 and CO (Fig. 5). These fragments are characteristic of TEA decomposition [35–37]. From EA it can be seen that carbon, hydrogen and nitrogen has roughly decreased to half their values at 300ºC. From the FTIR analysis of the solid residue at 450ºC it is impossible to distinguish the characteristic bands of TEA.

In a second stage between 450 and 650ºC we mainly observe the formation of ethylene oxide, N_2O, NH_3 and CO_2 (see in Fig. 5 the FTIR analysis of volatiles at 479ºC). The formation of N_2O can be attributed to the removal of the remaining NO_3 groups while the evolution of C_2H_4O, NH_3 and CO_2 indicate further degradation of the remaining fragments of TEA.

Finally, the decomposition is over at 800ºC. In between, we observe a new peak at 720ºC that corresponds to the pyrolysis of the carbonaceous residue and involves formation of NH_3, CO_2 and CO, related to the removal of the last fragments left behind by TEA. At 800ºC no carbon, hydrogen and nitrogen are detected beyond the sensibility of EA, while XRD analysis shows the presence of fluorite structure of CeO_2 (inset of Fig. 1).

Combined TG-EGA analysis performed in a 7.1 mg sample but in flowing air shows little differences: decomposition starts at the same temperature and the same volatiles are observed (CO is the single volatile absent because, in the presence of oxygen, it turns into CO_2). On the other hand, the presence of oxygen reduces the amount of TEA, because its oxidation in the gas phase is enhanced [37]. The most relevant effect of the presence of oxygen occurs at the last stages of decomposition. From Fig. 3 one can state that up to 290ºC the evolution of the decomposition in N_2 (6.2 mg) and air (7.1 mg) is nearly identical, but above this temperature, the decomposition is much faster in the presence of oxygen. Indeed, we have realized that the endset of the decomposition in inert atmosphere is not well defined. This is because the final degradation of the deprotonated TEA is mainly driven by residual oxygen [38]: the more inert the atmosphere, the longer the time to reach completeness. Using a lower flow of nitrogen to increase residual O_2 concentration or using smaller samples to prevent gas stagnation allows to complete the decomposition in a narrower temperature interval.

For sample masses above 8 mg, thermal runaway occurs in both N_2 and air. In both cases, the ratio between the mass after the thermal runaway and the initial mass is around 43% (Fig. 3). Therefore, and despite the high temperature achieved, decomposition is not complete. Probably, during the thermal runaway the decomposition is so fast that there is no time for O_2 to diffuse into the sample and, consequently, the evolution of the thermal runaway does not depend on the surrounding atmosphere but on the exothermic reaction between the components of the precursor: NO_3 that acts as oxidant and TEA as fuel. Therefore, once all NO_3 have evolved, the last stages of decomposition are probably sustained by oxygen. For this reason, the precursor is not fully decomposed after the thermal runaway; indeed, from Fig. 3 one can observe that in air the decomposition ends at 350ºC independently of the occurrence of a thermal runaway (this coincidence in the enset has been observed for 7 experiments of different initial masses ranging from 5 to 15 mg).

Finally, combined TG−EGA analysis of Ce−TEA−1 shows the same volatiles with the exception of TEA, which is not observed. Also, less nitrogen oxides are detected because of the lesser amount of NO_3; the mechanism of Ce−TEA−1 coincides with that of Ce−TEA−2 after TEA deprotonation.

4. Conclusions

The structure of Ce−TEA−2 is a network of $[Ce(NO_3)(C_6H_{15}NO_3)_2]^{2+}$ cations and two nitrate counter-ions. Decomposition of compound Ce−TEA−2 follows several stages and spans a temperature interval from 200ºC up to 350ºC in air or ends at higher temperatures in inert atmosphere.

The first decomposition stage takes place between 200 and 300ºC and involves the removal of a TEA molecule and two NO_3 groups. The remaining TEA achieves an atrane structure where cerium is strongly bonded to the deprotonated oxygen atoms of TEA. As a result, cerium changes its oxidations state from Ce(III) to Ce(IV). The main volatiles formed are TEA, H_2O, N_2O, NO and CO_2.

The second stage involves degradation of the deprotonated TEA and removal of the remaining NO_3 group. This stage is greatly enhanced by the presence of oxygen. Conversely, in inert atmosphere the decomposition rate depends on the amount of residual oxygen; depending on the inert conditions, decomposition can last up to 800ºC. The main volatiles formed are NH_3, C_2H_4O, N_2O, NO, CO and CO_2.

The structure of Ce−TEA−1 is a mixture of CeO_2 and the compound obtained after the first decomposition stage of Ce−TEA−2. Consequently, it decomposes essentially following the second decomposition stage of Ce−TEA−2.

For Ce−TEA−1 and Ce−TEA−2, if the sample mass is large enough, a thermal runaway occurs that results in a very fast decomposition. However, since the amount of oxygen released during decomposition is not enough to complete the second decomposition stage, after the thermal runaway, an organic residue remains. In air, the decomposition is complete at 350ºC wherever a thermal runaway occurs or not. In inert atmosphere, decomposition is shifted to higher temperatures but the occurrence of a thermal runaway significantly reduces the time needed to complete the decomposition; after the thermal runaway there is less organic fraction left so less oxygen is needed to completely remove it.

Acknowledgements

This work was funded by Ministerio de Ciencia, Innovación y Universidades (grant number RTI2018-095853-B-C22), by the Generalitat of Catalunya (2017-SGR-1519) and by the Universitat de Girona (UdG, contract number MPCUdG2016/059). The authors would like to thank Daniel Sánchez-Rodriguez for his insightful comments and advices in relation to this work.

References

[1] A. Trovarelli, P. Fornasiero, Catalysis by Ceria and Related Materials, 2nd editio, Imperial College Press, London, United Kingdom, 2013. doi:10.1142/p870.

[2] D. Sánchez-Rodríguez, S. Yamaguchi, D. Ihara, H. Yamaura, H. Yahiro, Self-propagating high-temperature synthesis of highly dispersed noble metals on ceria powder: Application to Pd/CeO 2 catalyst, Ceram. Int. 43 (2017) 14533–14536. doi:10.1016/j.ceramint.2017.07.208.

[3] E.P. Murray, T. Tsai, S.A. Barnett, A direct-methane fuel cell with a ceria-based anode, Nature. 400 (1999) 649–651. doi:10.1038/23220.

[4] N. Izu, W. Shin, N. Murayama, Fast response of resistive-type oxygen gas sensors based on nano-sized ceria powder, Sensors Actuators B Chem. 93 (2003) 449–453. doi:10.1016/S0925-4005(03)00167-9.

[5] B. Faure, G. Salazar-Alvarez, A. Ahniyaz, I. Villaluenga, G. Berriozabal, Y.R. De Miguel, L. Bergström, Dispersion and surface functionalization of oxide nanoparticles for transparent photocatalytic and UV-protecting coatings and sunscreens, Sci. Technol. Adv. Mater. 14 (2013) 023001. doi:10.1088/1468-6996/14/2/023001.

[6] P. Roura, J. Farjas, S. Ricart, M. Aklalouch, R. Guzman, J. Arbiol, T. Puig, A. Calleja, O. Peña-Rodríguez, M. Garriga, X. Obradors, Synthesis of nanocrystalline ceria thin films by low-temperature thermal decomposition of Ce-propionate, Thin Solid Films. 520 (2012) 1949–1953. doi:10.1016/j.tsf.2011.09.058.

[7] X. Zhong, Q. Li, J. Hu, Y. Lu, Characterization and corrosion studies of ceria thin film based on fluorinated AZ91D magnesium alloy, Corros. Sci. 50 (2008) 2304–2309. doi:10.1016/j.corsci.2008.05.016.

[8] R.K. Singh, R. Bajaj, Advances in Chemical-Mechanical Planarization, MRS Bull. 27 (2002) 743–751. doi:10.1557/mrs2002.244.

[9] A. Goyal, M.P. Paranthaman, U. Schoop, The RABiTS Approach: Using Rolling-Assisted Biaxially Textured Substrates for High-Performance YBCO Superconductors, MRS Bull. 29 (2004) 552–561. doi:10.1557/mrs2004.161.

[10] A. Calleja, R.B. Mos, P. Roura, J. Farjas, J. Arbiol, L. Ciontea, X. Obradors, T. Puig, Growth of epitaxial CeO2 buffer layers by polymer assisted deposition, MRS Proc. 1449 (2012) 31–39. doi:10.1557/opl.2012.1250.

[11] W. Chen, F. Li, J. Yu, Combustion synthesis and characterization of

nanocrystalline CeO2-based powders via ethylene glycol–nitrate process, Mater. Lett. 60 (2006) 57–62. doi:10.1016/j.matlet.2005.07.088.

[12] W. Wattanathana, A. Lakkham, A. Kaewvilai, N. Koonsaeng, A. Laobuthee, C. Veranitisagul, Preliminary Study of Pd/CeO2 Derived from Cerium Complexes as Solid Support Catalysts for Hydrogenation Reaction in a Micro-reactor, Energy Procedia. 9 (2011) 568–574. doi:10.1016/j.egypro.2011.09.066.

[13] D. Sanchez-Rodriguez, J. Farjas, P. Roura, S. Ricart, N. Mestres, X. Obradors, T. Puig, Thermal Analysis for Low Temperature Synthesis of Oxide Thin Films from Chemical Solutions, J. Phys. Chem. C. 117 (2013) 20133–20138. doi:10.1021/jp4049742.

[14] K.C. Patil, S.T. Aruna, T. Mimani, Combustion synthesis: an update, Curr. Opin. Solid State Mater. Sci. 6 (2002) 507–512. doi:10.1016/S1359-0286(02)00123-7.

[15] W. Wattanathana, C. Veranitisagul, S. Wannapaiboon, W. Klysubun, N. Koonsaeng, A. Laobuthee, Samarium doped ceria (SDC) synthesized by a metal triethanolamine complex decomposition method: Characterization and an ionic conductivity study, Ceram. Int. 43 (2017) 9823–9830. doi:10.1016/j.ceramint.2017.04.162.

[16] S. Kitagawa, M. Munakata, M. Ueda, 51V NMR studies of vanadium(I) complexes. Equilibria and crystal structure of Na[V(NO)(N(CH2CH2O)3)] and its derivatives, Inorganica Chim. Acta. 164 (1989) 49–53. doi:10.1016/S0020-1693(00)80874-9.

[17] J.W. Sharples, D. Collison, The coordination chemistry and magnetism of some 3d-4f and 4f amino-polyalcohol compounds, Coord. Chem. Rev. (2014). doi:10.1016/j.ccr.2013.09.011.

[18] P.S. Koroteev, A.B. Ilyukhin, N.N. Efimov, E. V. Belova, A. V. Gavrikov, V.M. Novotortsev, Mononuclear and binuclear lanthanide acetates with chelating and bridging triethanolamine ligands, Polyhedron. 154 (2018) 54–64. doi:10.1016/j.poly.2018.07.027.

[19] H. İçbudak, V.T. Yilmaz, H. Ölmez, Thermal decomposition behaviour of some trivalent transition and inner-transition metal complexes of triethanolamine, Thermochim. Acta. 289 (1996) 23–32. doi:10.1016/S0040-6031(96)03041-9.

[20] K. Majid, R. Mushtaq, S. Ahmad, Synthesis, Characterization and Coordinating Behaviour of Aminoalcohol Complexes with Transition Metals, E-Journal Chem. 5 (2008) S969–S979. doi:10.1155/2008/680324.

[21] A. Fowkes, W.T.A. Harrison, (Nitrato-κ 2 O , O ′)bis(triethanolamine-κ 4 N , O , O ′, O ″)lanthanum(III) dinitrate, Acta Crystallogr. Sect. C Cryst. Struct. Commun. 62 (2006) m232–m233. doi:10.1107/S0108270106011826.

[22] I. Mylonas-Margaritis, J. Mayans, S.-M. Sakellakou, C. P. Raptopoulou, V. Psycharis, A. Escuer, S. P. Perlepes, Using the Singly Deprotonated Triethanolamine to Prepare Dinuclear Lanthanide(III) Complexes: Synthesis, Structural Characterization and Magnetic Studies, Magnetochemistry. 3 (2017) 5. doi:10.3390/magnetochemistry3010005.

[23] H. Içbudak, V.T. Yilmaz, H. Ölmez, Thermal decompositions of some divalent transition metal complexes of triethanolamine, J. Therm. Anal. Calorim. 44 (1995) 605–615. doi:10.1007/BF02636280.

[24] Y. Kondratenko, V. Fundamensky, I. Ignatyev, A. Zolotarev, T. Kochina, V. Ugolkov, Synthesis and crystal structure of two zinc-containing complexes of triethanolamine, Polyhedron. 130 (2017) 176–183. doi:10.1016/j.poly.2017.04.022.

[25] A.A. Naiini, V. Young, J.G. Verkade, G. Hall, New complexes of thriethanolamine (Tea): Novel structural features of [Y(TEA)2](ClO4)3·3C5H5N and [Cd(TEA)2](NO3)2, Polyhedron. 14 (1995) 393–400. doi:10.1016/0277-5387(95)93020-2.

[26] K.H. Whitmire, J.C. Hutchison, A. Gardberg, C. Edwards, Triethanolamine complexes of copper, Inorganica Chim. Acta. 294 (1999) 153–162. doi:10.1016/S0020-1693(99)00274-1.

[27] W. Wattanathana, N. Nootsuwan, C. Veranitisagul, N. Koonsaeng, N. Laosiripojana, A. Laobuthee, Simple cerium-triethanolamine complex: Synthesis, characterization, thermal decomposition and its application to prepare ceria support for platinum catalysts used in methane steam reforming, J. Mol. Struct. 1089 (2015) 9–15. doi:10.1016/j.molstruc.2015.02.010.

[28] V.. Yilmaz, Y. Topcu, A. Karadag, Thermal decomposition of triethanolamine and monoethanolethylenediamine complexes of some transition metal saccharinates, Thermochim. Acta. 383 (2002) 129–135. doi:10.1016/S0040-6031(01)00685-2.

[29] K. LIU, M. ZHONG, Synthesis of monodispersed nanosized CeO2 by hydrolysis of the cerium complex precursor, J. Rare Earths. 28 (2010) 680–683. doi:10.1016/S1002-0721(09)60178-2.

[30] R.K. Pati, I.C. Lee, K.J. Gaskell, S.H. Ehrman, Precipitation of Nanocrystalline CeO 2 Using Triethanolamine, Langmuir. 25 (2009) 67–70. doi:10.1021/la8031286.

[31] D.G. Brannon, R.H. Morrison, J.L. Hall, G.L. Humphrey, D.N. Zimmerman, Spectra and bonding for copper(II)-aminoalcohol complexes—I, J. Inorg. Nucl. Chem. 33 (1971) 981–990. doi:10.1016/0022-1902(71)80164-1.

[32] D. Sánchez-Rodriguez, J. Farjas, P. Roura, The critical condition for thermal explosion in an isoperibolic system, AIChE J. 63 (2017) 3979–3993. doi:10.1002/aic.15727.

[33] D. Sánchez-Rodriguez, J. Farjas, P. Roura, The critical conditions for thermal explosion in a system heated at a constant rate, Combust. Flame. 186 (2017) 211–219. doi:10.1016/j.combustflame.2017.08.008.

[34] A.G. Merzhanov, V.V. Barzykin, A.S. Shteinberg, V.T. Gontkovskaya, Methodological Principles in studying chemical reaction kinetics under conditions of programmed heating, Thermochim. Acta. 21 (1977) 301–332. doi:10.1016/0040-6031(77)85001-6.

[35] S.G. de Ávila, M.A. Logli, J.R. Matos, Kinetic study of the thermal decomposition of monoethanolamine (MEA), diethanolamine (DEA), triethanolamine (TEA) and methyldiethanolamine (MDEA), Int. J. Greenh. Gas Control. 42 (2015) 666–671. doi:10.1016/j.ijggc.2015.10.001.

[36] H.A. Schwarz, Chain decomposition of aqueous triethanolamine, J. Phys. Chem. 86 (1982) 3431–3435. doi:10.1021/j100214a033.

[37] I. Zghal, J. Farjas, J. Camps, M. Dammak, P. Roura, Thermogravimetric measurement of the equilibrium vapour pressure: Application to water and triethanolamine, Thermochim. Acta. 665 (2018) 92–101. doi:10.1016/j.tca.2018.05.007.

[38] P. Roura, J. Farjas, J. Camps, S. Ricart, J. Arbiol, T. Puig, X. Obradors, Decomposition processes and structural transformations of cerium propionate into nanocrystalline ceria at different oxygen partial pressures, J. Nanoparticle Res. 13 (2011) 4085–4096. doi:10.1007/s11051-011-0352-9.

[39] N.C. Anastasiadis, D.A. Kalofolias, A. Philippidis, S. Tzani, C.P. Raptopoulou, V. Psycharis, C.J. Milios, A. Escuer, S.P. Perlepes, A family of dinuclear lanthanide(<scp>iii</scp>) complexes from the use of a tridentate Schiff base, Dalt. Trans. 44 (2015) 10200–10209. doi:10.1039/C5DT01218J.

[40] W. Haron, T. Thaweechai, W. Wattanathana, A. Laobuthee, H. Manaspiya, C. Veranitisagul, N. Koonsaeng, Structural Characteristics and Dielectric Properties of La1-xCoxFeO3 and LaFe1-xCoxO3 Synthesized via Metal Organic Complexes, Energy Procedia. 34 (2013) 791–800. doi:10.1016/j.egypro.2013.06.815.

[41] W. Wallace, Infrared spectra, in: P.J. Linstrom, W.G. Mallard (Eds.), NIST Chem. WebBook, NIST Stand. Ref. Database, Institute of Standards and Technology, Gaithersburg MD, 2019: p. 20899. doi:10.18434/T4D303.

Table 1. Weight percentages determined from Elemental Analysis of Ce−TEA−2 as-grown and quenched at different temperatures. In parentheses calculated values for $[Ce(NO_3)(C_6H_{15}NO_3)_2](NO_3)_2$.

Temperature (ºC)	**C wt%**	**H wt%**	**N wt%**
As grown	23.2 (23.08)	4.7 (4.80)	10.6 (11.21)
225ºC	21.7	4.3	10.4
250ºC	23.1	3.5	10.5
260ºC	25.6	2.7	9.0
280ºC	26.3	2.4	7.6
300ºC	22.6	2.1	6.2
450ºC	15.5	1.0	3.8

Table 2. FTIR assignments of compounds Ce−TEA−1 and Ce−TEA−2.

Ce−TEA−2 Wavenumber cm^{-1}	Ce−TEA−1 Wavenumber cm^{-1}	Assignment
3157		−OH stretch [22,31]
2990, 2970, 2908, 2855	2960, 2895, 2855	C−H stretch
1641, 1596		−OH bend [22]
1460, 1435		N=O stretch [31,39]
	1413	NO_3^- stretch
1378	1373	$-CH_2-$ bend
1325		O−H in plane bend
1290		N−O stretch [39]
	1301	NO_3^- stretch
1153	1153	C−N [40]
1061	1065	C−C−O asym. stretch [31]
1030		C−C−O sym. stretch [39]
898		C−N stretch
817		NO_3^- bend
735		CH_2 bend
667		O−H bend
	462	Ce−O

Table 3. Weight percentages determined from Elemental Analysis of Ce−TEA−1. In parentheses calculated values for the mixture Ce $(C_6H_{12}NO_3)(NO_3)_{1.21}$ + 0.56 CeO_2.

C wt. %	**H wt. %**	**N wt. %**
15.7	2.45	6.8
(15.7)	(2.57)	(6.8)

Figure captions

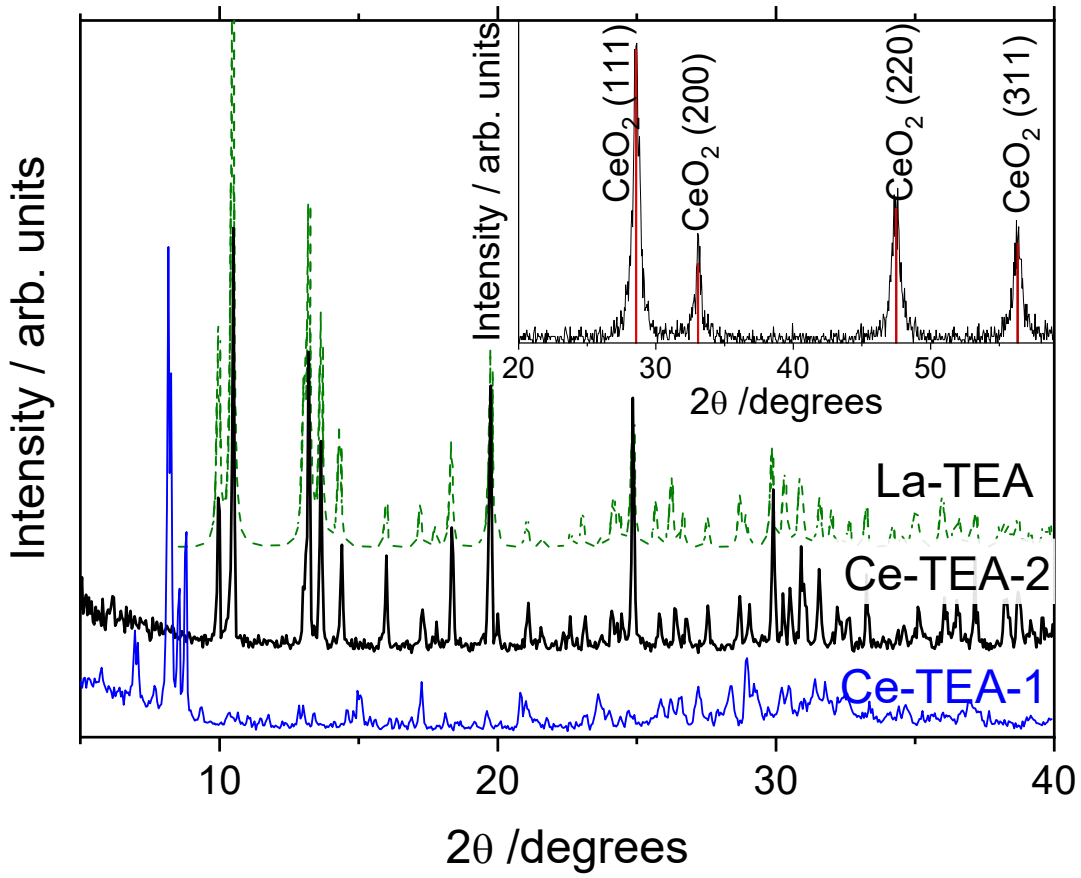

Fig. 1. XRD diffraction curves of Ce−TEA−1, Ce−TEA−2 and La−TEA [21]. Inset: diffraction curves of Ce−TEA−2 after heating up to 800ºC at 10 K/min in N_2 flowing atmosphere. The bars correspond to the cubic fluorite structure of CeO_2 (JCPDS pattern PDF 43-1002).

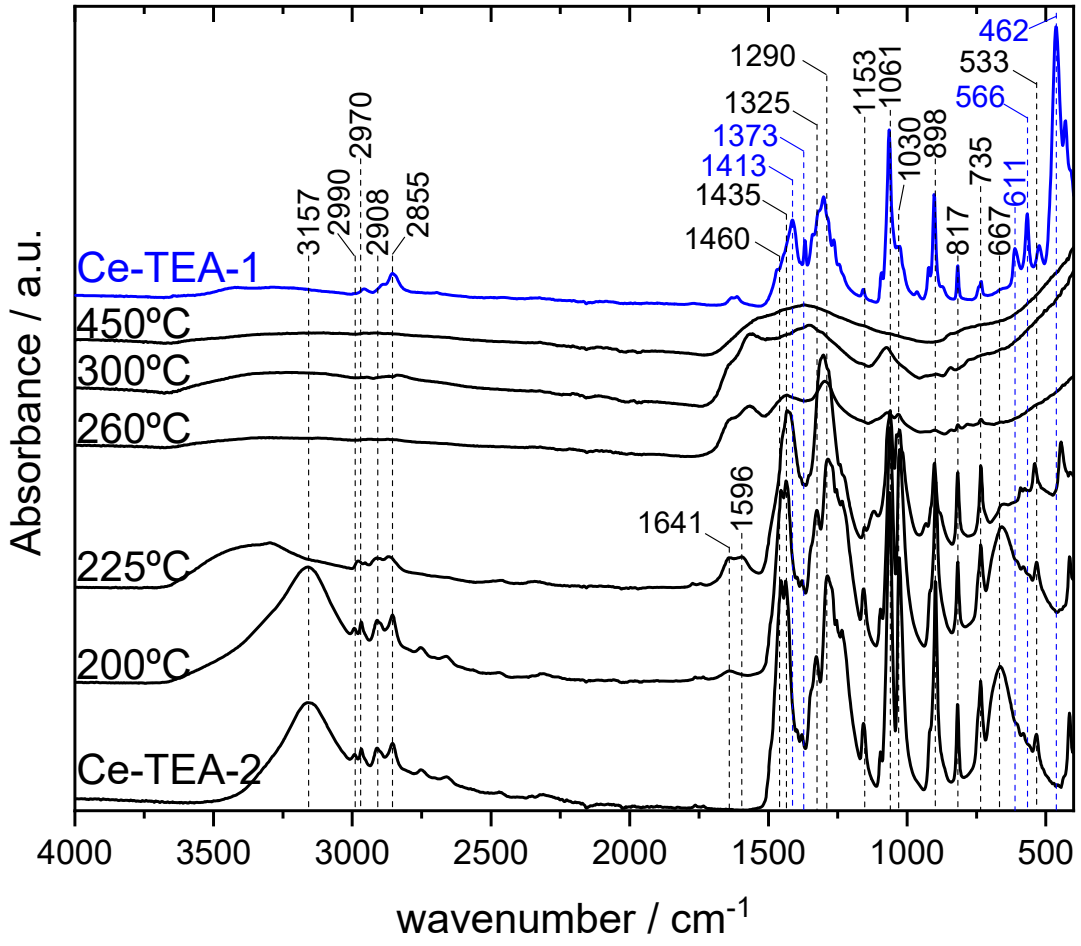

Fig. 2. FTIR spectra of as-grown Ce−TEA−1 (top blue curve) and Ce−TEA−2 (rest of curves, black) as grown (bottom curve) and after heating it at 10 K/min in N_2 flow up to a given temperature. Sample masses are around 6 mg to prevent the event of a thermal runaway.

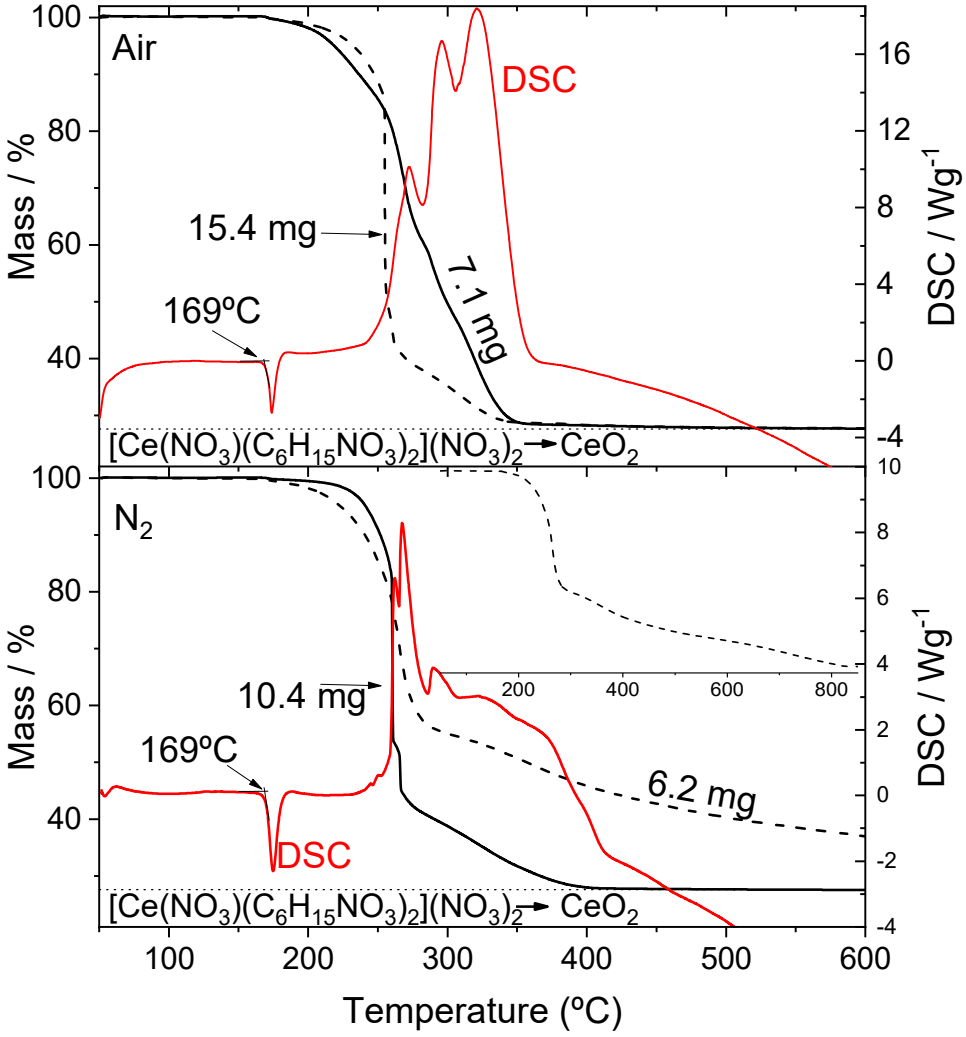

Fig. 3. TG curves of Ce−TEA−2 heated at 10 K/min under flowing synthetic air (top) or N_2 (bottom) and simultaneous DSC of the samples of initial masses 7.1 mg and 10.4 mg. Horizontal dotted line: expected mass for the conversion of $[Ce(NO_3)(C_6H_{15}NO_3)_2](NO_3)_2$ into CeO_2. Inset: complete evolution of the sample of initial mass 6.2 mg.

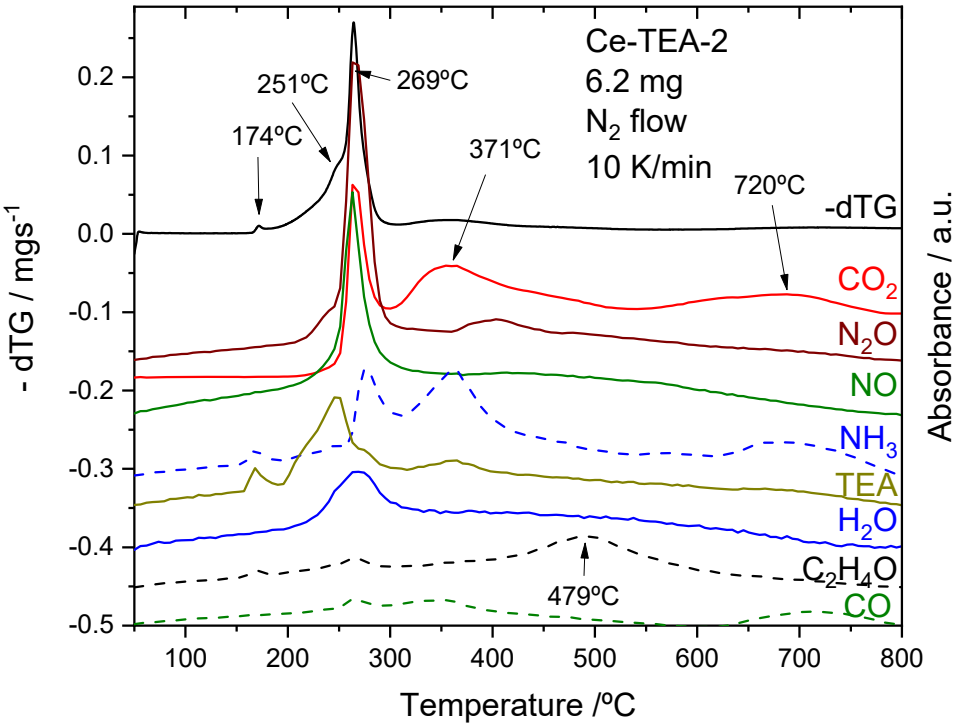

Fig. 4. Transformation rate (−dTG) of the sample of 6.2 mg of Fig. 3 together with the evolution of the intensity of the absorption peaks representative of the main volatiles detected during Ce−TEA−2 decomposition: CO_2 (2360 cm^{-1}), N_2O, (2239 cm^{-1}), NO (1845 cm^{-1}), NH_3 (964 cm^{-1}), TEA (1075 cm^{-1}), CO (2116 cm^{-1}), H_2O (3903 cm^{-1}) and C_2H_4O (3015 cm^{-1}). EGA signal of CO_2 has been divided by a factor 5. FTIR spectra at the indicated selected temperatures are shown in Fig. 5.

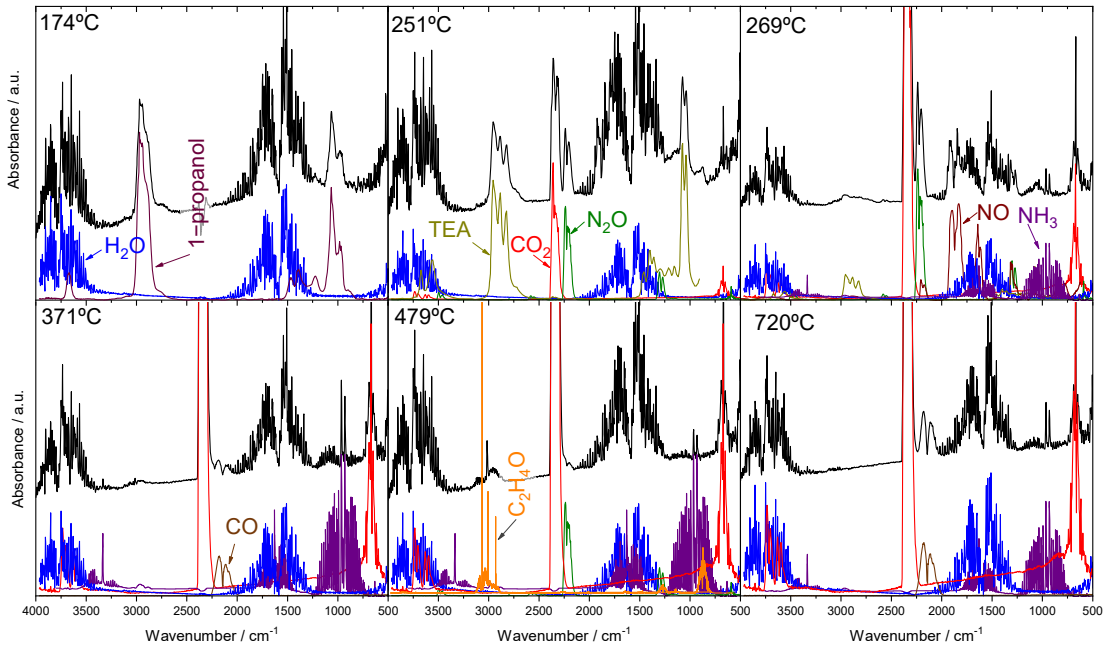

Fig 5. Top shifted curves (black lines) are selected FTIR spectra of the volatiles evolved during the TG experiment of Fig. 3 (mass 6.2 mg) and Fig. 4. Bottom curves are reference spectra obtained from the NIST library [41] except the TEA spectrum that has been obtained in our laboratory [37].

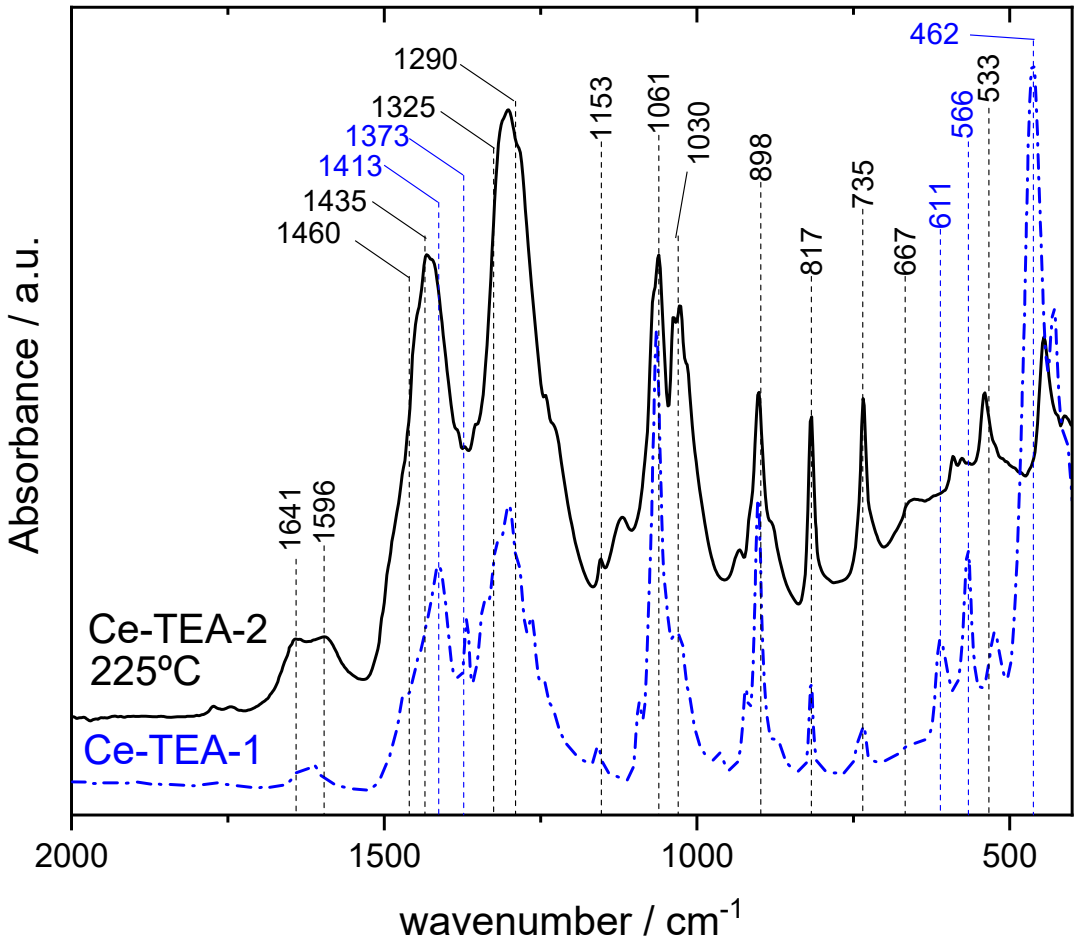

Fig. 6. Comparison between the FTIR spectra of as-grown Ce−TEA−2 (solid) and Ce−TEA−1 (dashed) after heating it at 10 K/min in N_2 flow up to 225ºC.